ACS OMEGA

Open Access

http://pubs.acs.org/journal/acsodf

Article

Reaction Properties of Basic Oxygen Furnace Slag and Methane in a Fluidized-Bed Chemical Looping System

Cetera Chen,* Seng-Rung Wu, and Ching-Ti Kao

Cite This: *ACS Omega* 2023, 8, 47075−47085

Read Online

ACCESS | Metrics & More | Article Recommendations

ABSTRACT: In the conventional steelmaking process, slag is the second-largest byproduct. Although most slags have ways to be reused, the demand for small BOF (basic oxygen furnace) slag is still limited. This study aimed to develop a fluidized-bed chemical looping system using BOF slag as an oxygen carrier and methane as a fuel to produce heat for the steelmaking process. The results of the BOF slag reaction test on a batch fluidization and reaction test facility indicated that the methane conversion rate increased with an increase in the methane concentrations and the reaction temperature. As methane concentration increased from 5 to 15 v/v % at the reaction temperature of 950 °C and the fluidized velocity of 5.1 times the minimum fluidized velocity of BOF slag, the methane conversion rate increased from 65.8 to 76.6%. By setting 10 v/v % as the referenced methane concentration, the methane conversion rate corresponded to 71.6%, and as the reaction temperature increased to 980 °C, the methane conversion rate of 85.7% was achieved. The fluidized gas velocity influenced the fluidized state of the oxygen carrier and the gas residence time in the reactor. As the gas velocity was 1.9 times the minimum fluidization velocity of BOF, the methane and oxygen carrier conversion rates reached 83.3 and 13.0% at the referenced methane concentration and reaction temperature of 950 °C. The experimental results could offer the required design and operation parameters for the methane fluidized bed chemical looping system using BOF slag as the oxygen carrier.

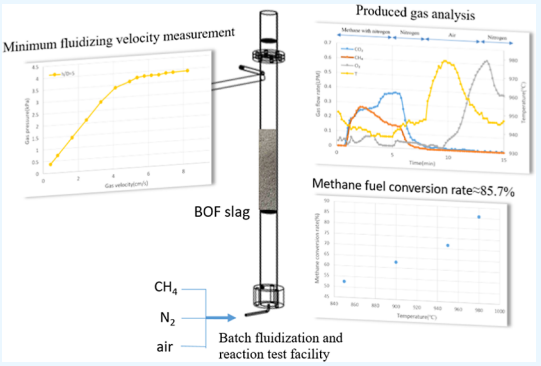

1. INTRODUCTION

The global warming effect causes extreme climate change and threatens life on earth. In order to reduce the impact of the effect on human society, the United Nations Framework Convention on Climate Change (UNFCCC) integrates nations' efforts to decrease the emission of greenhouse gases, especially CO_2. In Taiwan (R.O.C.), the government passed the Greenhouse Gas Reduction and Management Action Act in 2015[1] and set the target for 2050 to be net zero emissions of global greenhouse gases.

For Taiwan's industry, the energy, cement, and metal industries contributed to the main annual carbon emissions. Consequently, the companies in these industries have a large responsibility to reduce Taiwan's carbon emissions. To meet the reduction requirement for carbon emissions, CO_2 capture and adsorption technology will be used to separate CO_2 from flue gas. But the post-carbon capture system consumes a large amount of energy for the adsorption and desorption of CO_2[2] and then causes a decrease in factory production efficiency.[3] Different from gas separation carbon capture technology, chemical looping technology offers a process to produce heat or hydrogen and to accomplish the capture of high concentrations of CO_2[4−6] which can be stored or used at a low cost.[7]

In the conventional steelmaking process, molten pig iron is used to produce steel in a basic oxygen furnace (BOF) (also called a Linz-Donawitz converter). Limestone, dolomite, and other raw materials are added to the BOF during steelmaking. The impurities in these molten raw materials constitute BOF slag, the second-largest byproduct in steelmaking. Subsequently, the BOF slag is removed to form molten steel. BOF slag has a high lime content, and therefore, it reacts with water to produce calcium hydroxide and expands in volume, thereby limiting its reuse.

Less than half of BOF slag is recirculated in the basic oxygen furnace; most of it is reused in road construction.[8] However, the demand for BOF slag with small particles (<5 mm) is very limited, thus necessitating an additional depleting process, which increases the cost and carbon footprint of the steelmaking process. BOF slag mainly contains Ca (30−40 wt %), Fe (∼20 wt %), Si (∼15 wt %), and Al (∼6 wt %).[9,10] The iron in BOF

Received: September 12, 2023
Revised: November 1, 2023
Accepted: November 10, 2023
Published: November 28, 2023

slag and other byproducts from steel production is considered the active element to serve as an oxygen carrier in a chemical looping system for heat and hydrogen production.[11−13] Consequently, the use of BOF slag as an oxygen carrier in the chemical looping process offers an effective reuse method for small particles of BOF slag. The heat energy and hydrogen produced from the chemical looping system could supply part of the energy requirement for the steelmaking process and also reduce the carbon emissions of the steelmaking plant at a lower cost. The cost effect of the oxygen carrier showed more significance for the chemical looping system with solid fuel since the lifetime of the oxygen carrier decreased due to the deactivation of the oxygen carrier by the ash produced from the reaction of solid fuel (Linderholm et al., 2012; Hildor et al., 2020).[14,15]

The Chalmers research group[16,17] utilized BOF slag as an oxygen carrier for combustion in a 12MW_{th} biomass CFB boiler. From the result, a slight reactivity decay of material was observed, but the particle size of the BOF slag oxygen carrier was kept during the test without any particle agglomeration, and fuel conversion was promoted compared to only silica sand used as the bed material.

A Swedish research group used BOF slag as an oxygen carrier in tests with 300-W_t and 10 kW_t fluidized-bed chemical looping systems.[18] In the test of the 10 kW_t system, steam-exploded pellets and wood char were used as solid fuels. The fuel conversion rate was found to be approximately 75%, and wood char achieved a better fuel conversion at 92%. In a test of the 300-W_t system, methane and syngas were used as fuel, and at a reaction temperature of 900 °C, 99.9% of syngas was converted into CO_2. At a reaction temperature of 950 °C, the methane conversion rate was 60%. In the other redox test on a batch fluidized bed performed by Mattison et al., synthetic gasification gases, including CO, H_2, CH_4, C_2H_4, and C_6H_6, as well as reducing gases, showed lower methane conversion at 900 °C.[19,20]

For the specific physical and reaction properties of BOF slag, the objective of this study was to design a methane fluidized bed chemical looping system using BOF slag as the oxygen carrier and determine the system operation parameters. Thus, a process design for a fluidized bed chemical looping system of BOF slag and methane was arranged. And cold mold and hot mold experiments were conducted on a batch fluidized-bed reaction test facility in this work to investigate the effects of operation parameters, such as methane concentration, reaction temperature, and velocity of fluidized gas, on the fluidization reaction properties of BOF slag and methane.

2. TREATMENT AND PROPERTIES OF BOF SLAG

BOF slag obtained from China Steel Corporation (CSC) was used as the oxygen carrier (Figure 1). The raw slag was dried, crushed, and sieved to obtain particles with diameters of 177−297 μm for the fluidized chemical looping experimental test.

An X-ray fluorescence (XRF) oxide composition analysis of the CSC slag particles indicated that the main components were CaO (45.3 wt %) and Fe_2O_3 (21.6 wt %) (Table 1).

The oxygen content of BOF slag was determined by a thermogravimetric analyzer (TGA, Setaram). The gas used for the reduction process was 20% H_2 and 80% N_2, and air was used for the oxidation process. The durations of the reduction and oxidation reactions were set to 40 and 10 min, respectively, while the oxygen carrier (100 mg) was heated to 850 °C. The oxygen

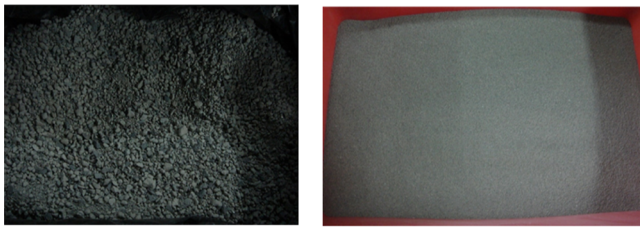

(a) (b)

Figure 1. BOF slag, (a) raw material, and (b) processed material.

content of material ($X_{oxygencontent}$) can be obtained from the weight data of particles using the following equations

$$X_{oxygencontent}(\%) = \frac{W_{oxi} - W_{red}}{W_{oxi}} \quad (1)$$

where W_{oxi} is the sample mass in a fully oxidized state, and W_{red} is the sample mass in the reduced form. The 50 cycles TGA test results of the oxygen content of BOF slag with a diameter between 177−297 μm are shown in Figure 2. In the TGA test, the oxygen release sharply rose to approximately 6% in 3 cycles and then increased slightly close to the theoretical oxygen release value (6.48%) of used BOF slag with the testing cycles. After 50 redox cycles, no obvious sintering of the BOF slag test sample was observed.

The slight increase of oxygen release of BOF slag with the redox cycle implies the activation of the material, which can account for the Fe_2O_3 diffusion to the surface of particles. During the redox process of metal alloy particles, the difference of diffusion rates of metal ions make them more active, gradually transporting them to the particle surface and increasing the reactivity of the oxygen carrier. The so-called phase separation effect was experimentally observed in Fe−Ni−O, Fe−Ti−O, and Fe−Zr−O composite.[21−23] In this work, BOF slag mainly contains Ca, Fe, Si, Mg, and Al, and the detailed microstructure transformation of such metal composites through the phase separation effect should be investigated in further research.

3. MINIMUM FLUIDIZATION VELOCITY OF BOF SLAG

This study used BOF slag as the oxygen carrier in the chemical looping system. To understand the reaction properties between the slag and methane for the design of the chemical looping reaction system, fluidization and reaction experiments for slag were conducted in an oxygen carrier fluidization and reaction test facility.

3.1. Test Facility. The oxygen carrier fluidization and reaction test facility is a batch fluidized-bed reactor system. Through the switching of the input gas, the reducing and oxidizing reactions of the oxygen carrier were alternately performed for a specific period in one system. As fuel was introduced into the reactor, the oxygen carrier was reduced. At the end of the reduction period, nitrogen was introduced as an inert gas into the reactor to clear the gas in the reactor. Subsequently, air was injected as an oxidizing gas to oxidize the oxygen carrier. After the oxidizing reaction, the reactor was cleared and purged using nitrogen; thereafter, the subsequent reduction−oxidization cycle was performed.

The main body of the reactor of the test facility was composed of a stainless steel 310 tube with an inner diameter of 5 cm and a height of 80 cm (Figure 3). The system was heated up by an electric heater, and the input gas flow rate was controlled by a gas mass flow controller. The gas was introduced to fluidize the

https://doi.org/10.1021/acsomega.3c03390
ACS Omega 2023, 8, 47075−47085

Table 1. Oxide Composition of BOF Slag

composition	CaO	Fe_2O_3	SiO_2	MgO	Al_2O_3	MnO	P_2O_5	other (S, TiO_2, and Cr_2O_5)
weight percentage (%)	45.3	21.6	11.5	6.4	5.3	4.0	1.9	3.9

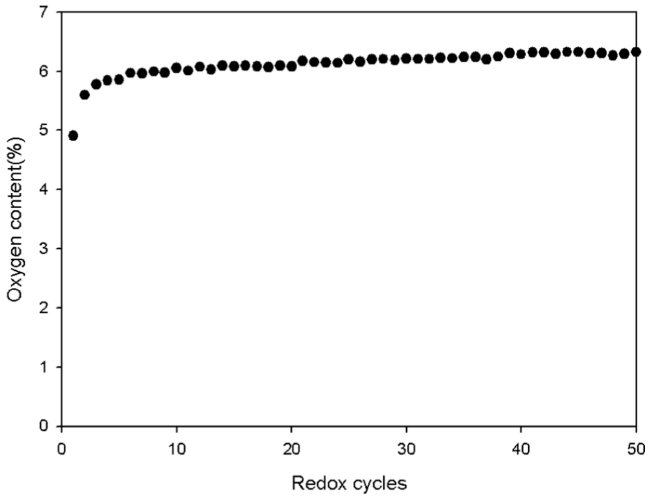

Figure 2. Oxygen content of BOF slag measured by the TGA redox cycling test.

Figure 3. Fluidization reaction reactor: (A) top section of reactor, (B) gas sampling tube, (C) supporting beam, (D) reactor body, and (E) fluidized gas input tube.

oxygen carrier through a 150 mesh metal net at the bottom of the reactor. The reaction pressure and temperature of the oxygen carrier at the bottom of the reactor were monitored by a pressure transducer and a K-type thermocouple extended into the bed.

The produced gases were exhausted and sampled from the top of the reactor. A nondispersive infrared gas analyzer was used to measure the concentrations of CO_2, CH_4, CO, H_2 (heat conductivity), and O_2 (electrochemical) gas species.

The methane conversion rate X_{CH_4} is defined as follows

$$X_{CH_4} = \frac{C_{FR,CO} + C_{FR,CO_2}}{C_{FR,CO} + C_{FR,CO_2} + C_{FR,CH_4}} \times 100\% \quad (2)$$

where $C_{FR,i}$ is the volume fraction of the exhaust gas species in the fuel reactor (v/v %), and i is an index representing the gas species CO, CO_2, or CH_4.

At the end of the test, the BOF slag oxygen carrier was reduced by a single reducing process. Subsequently, the oxygen carrier was cooled through the purging of nitrogen in the reactor. Thereafter, a sample of the reduced oxygen carrier was analyzed using TGA (Setaram) and X-ray diffraction (XRD, Bruker). The state of iron oxide was determined using XRD analysis. Parts of the reducing oxygen carrier were oxidized in an oven in air at 600 °C; these served as the oxidizing sample. Then, the Fe_2O_3 content in the oxidation sample was estimated. In eq 3, m_{OC} is the weight of the oxygen carrier of the BOF slag, m_o is the mass of the iron sample in the fully oxidized state, and $f_{Fe_2O_3}$ is the Fe_2O_3 weight percentage in the oxidation sample, as determined using XRF analysis of the BOF slag oxygen carrier.

$$m_o = m_{OC} \times f_{Fe_2O_3} \quad (3)$$

In the TGA test, the reduced sample was oxidized by air, and from the weight increase and Fe_2O_3 concentration as analyzed by XRF, the conversion rate of the oxygen carrier (X_{OC}) was evaluated as

$$X_{OC} = \frac{m_o - m_{r,t}}{m_o - m_r} \times 100\% \quad (4)$$

where m_r is the mass of the iron sample in reduced form, and $m_{r,t}$ is the mass of the iron sample after the reaction with the reducing fuel.

3.2. Measurement of Minimum Fluidization Velocity (U_{mf}) of BOF Slag. The minimum fluidization velocity is a basic parameter for the design and operation of the fluidization and reaction systems. In this study, the minimum fluidization velocity (U_{mf}) of the BOF slag was measured by using the oxygen carrier fluidization and reaction test facility. The fluidization velocity was the superficial velocity of the introduced air, as calculated from the gas flow rate. Figure 4 illustrates the fluidization velocity of particles with the bottom pressure of the fluidized bed. At a small fluidization velocity, the pressure at the bottom of the reactor increased linearly with the fluidization velocity. When the velocity was large enough, the pressure increased slowly with velocity at a flat slop. U_{mf} was defined as the value of the velocity at which the extrapolations of the two sloped lines intersect.

In the study, the influence of the ratio of the oxygen carrier bed height (h) to the reactor diameter (D) on the U_{mf} of the BOF slag was tested using compressing air as fluidizing gas at ambient conditions (Figure 5). At h/D values of 0.5, 1, and 2, U_{mf} was 3.7 cm/s. As the gas velocity further increased, the pressure at the bottom of the reactor remained almost constant. In addition, the pressure increased with the value of h/D, owing to the weight effect of the oxygen carrier. As h/D increased to 5, U_{mf} was observed to increase to 4.4 cm/s.

The minimum fluidized velocity of the particle was mainly influenced by the density, size, and viscosity of the particle and gas[24,25] and can be calculated from the following equation

https://doi.org/10.1021/acsomega.3c03390
ACS Omega 2023, 8, 47075−47085

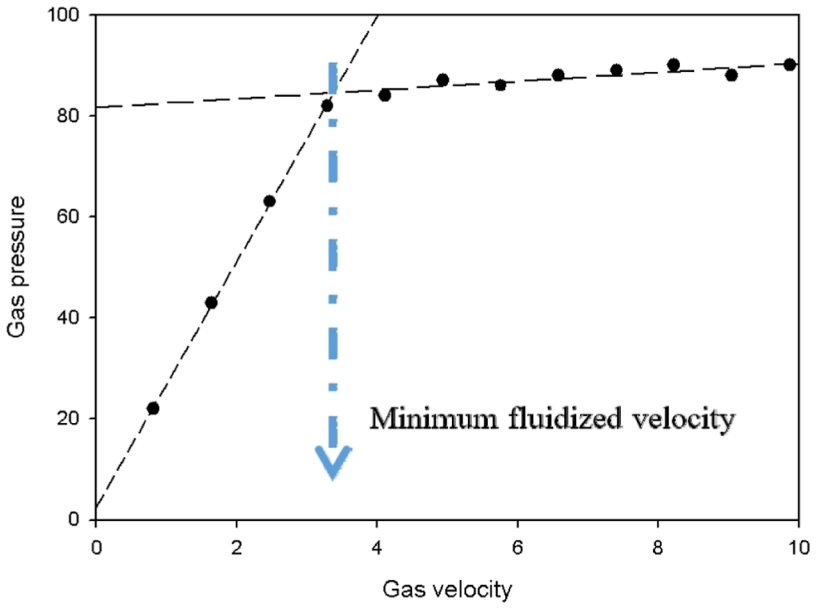

Figure 4. Schematic of the fluidization velocity of the particle with fluidized-bed bottom pressure.

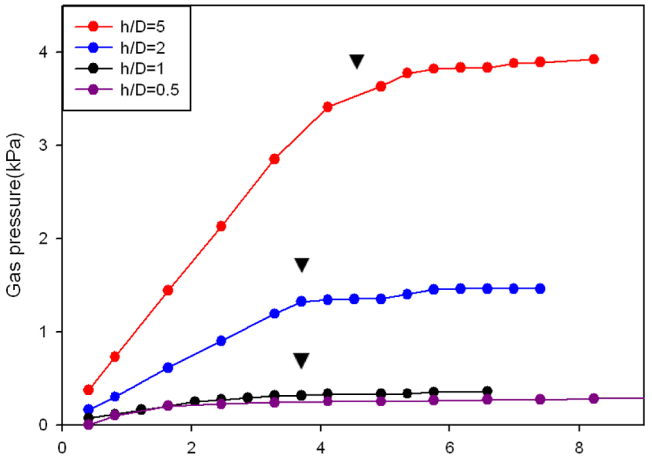

Figure 5. Relation between gas velocity and pressure at the bottom of the reactor at different h/D values of BOF slag (▼:U_{mf}).

$$150(1-\varepsilon)^2 U_{mf} + 1.75(1-\varepsilon)\frac{\rho_g \varphi d_p}{\mu_g} U_{mf}^2 = \frac{g\varepsilon^3 \varphi^2 d_p^2 (\rho_p - \rho_g)}{\mu_g} \quad (5)$$

where ε is particles' voidage, ρ_g is gas density in kg/m^3, ρ_p is particle true density in kg/m^3, d_p is solid particle's diameter in m, φ is particle sphericity, and μ_g is gas viscosity in Pa·s.

Besides, there are other studies presenting that the wall effect of the fluidized bed chamber wall also effects the minimum fluidized velocity of the particle by the vertical stress between the chamber wall and the fluidized materials, especially in the case of the micro-fluidized bed, referring to the bed inner diameter of a few millimeters. The experimental results indicated that the smaller diameter of the chamber facilitated the wall effect and provided the minimum fluidized velocity. Apart from the chamber diameter, the bed height also positively contributes to the wall friction caused by the material weight and the fluidizing drag force of particles. In Liu et al.'s experimental study,[26] the minimum fluidized velocity slightly increased as h/D increased up to 5, which was consistent with the observing result of this work. Rao et al. concerned the wall stress effect in the minimum fluidized velocity simulation model, and the calculating predictions were compared favorably to Liu et al.'s experimental measurements.[27]

3.3. Process Design of the Fluidization Reaction between BOF Slag and Methane. In the fluidized bed, as the gas velocity was 3−6 times U_{mf}, the fluidization phenomenon of the oxygen carrier featured bubble fluidization. According to the U_{mf} measuring results in Section 3.2 of this work, as the h/D value of the BOF slag oxygen carrier was below 2, the U_{mf} of the BOF slag was 3.7 cm/s. When the fluidized gas velocity was maintained at 6 times the minimum fluidizing velocity of the BOF slag at a reaction temperature of 950 °C, the gas flow rate in the tubular reactor with an inner diameter of 5 cm was calculated to be 6.4 LPM.

As methane was used as fuel, its concentration should be below 20% to avoid its decomposition at a high temperature[28] and the resultant deposition of solid carbon in the reactor. In this study, methane concentration was set at 10%, corresponding to a flow rate of 0.65 LPM (0.026 mol at 25 °C) at an input total flow rate of 6.5 LPM, and the remaining gas was nitrogen. According to the TGA test result of iron oxide material in a mixture containing 20% hydrogen gas, the reduction reaction was set to take 5 min to reduce the oxidized state of Fe_2O_3 to the oxidized state of Fe_3O_4. At a reaction time of 5 min, 0.13 mol of methane was input into the reactor, and thus, 249.6 g of Fe_2O_3 was required to provide sufficient oxygen while methane was converted into CO_2 and Fe_3O_4 was produced (eq 6).

$$12Fe_2O_3 + CH_4 \rightarrow 8Fe_3O_4 + CO_2 + 2H_2O \quad (6)$$

Owing to a Fe_2O_3 content of 21.6 wt % in BOF slag, the filling amount of BOF slag in the reactor was 1155.6 g, and with a BOF slag bulk density of 1.6 g/cm^3, the filling amount of BOF slag was 722.2 cm^3. In the tubular reactor with an inner diameter of 5 cm, the filling height of the BOF slag oxygen carrier was 36.8 cm, and h/D was 7.4. For fluidization operation, a h/D of 7.4 is too high to affect fluidizing motion. Consequently, a h/D of 5, corresponding to 490.6 cm^3 of BOF slag filling amount and a

https://doi.org/10.1021/acsomega.3c03390
ACS Omega 2023, 8, 47075−47085

Fe_2O_3 content of 169.6 g (1.06 mol), was adopted for experimental operation, and the U_{mf} of BOF slag was revised to 4.4 cm/s. At a gas flow rate of 6.5 LPM, the gas velocity was almost 5.1 times the U_{mf} of BOF slag.

According to the reaction of methane and oxygen (eq 7) and the 0.65 LPM input flow rate of methane in the reduction reaction, the oxygen supply rate should be greater than 1.3 LPM in the oxidation reaction, corresponding to 5.2 LPM of air.

$$CH_4+2O_2\rightarrow CO_2+2H_2O \quad (7)$$

4. RESULTS AND DISCUSSION

The reducing and oxidizing reaction tests of the BOF slag were alternately performed in a batch fluidization and reaction test facility, and methane diluted with nitrogen was introduced as the fuel. The effects of methane concentration, reaction temperature, and fluidization velocity on the reaction of the BOF slag and methane were investigated to evaluate the operational design of the interconnected fluidized-bed chemical looping system. Table 2 lists the experimental conditions. Among the tests in this work, test 1 was considered a reference test.

Table 2. Conditions of BOF Slag Reaction Experiments

	methane concentration (v/v %)	reaction temperature (°C)	gas flow rate (LPM, at 28 °C)	gas superficial velocity (cm/s)
test 1 (reference test)	10	950	6.5	22.5
test 2	5	950	6.5	22.5
test 3	15	950	6.5	22.5
test 4	10	850	6.5	20.7
test 5	10	900	6.5	21.6
test 6	10	980	6.5	23.1
test 7	10	950	5.0	17.3
test 8	10	950	3.0	10.4

4.1. Effect of Methane Concentration. For the fluidization reaction test for oxidation and reduction of the BOF slag, BOF slag with volumes and weights of 490 cm^3 and 784 g, respectively, was filled in the reactor. Consequently, the height of the oxygen carrier in the reactor was 25 cm, corresponding to an h/D value of 5. The reaction temperature was set at 950 °C. The total input gas flow rate was 6.5 LPM, and the methane flow rate was set to 0.65 LPM to control the methane concentration to 10v/v %. The reaction time in each reducing and oxidizing sequence was 5 min, and nitrogen was purged between the reducing and oxidizing sequences for 3 min. The CO_2, CH_4, CO, H_2, and O_2 flow rates in the exhaust gas (Figure 6a) were estimated from their respective species concentrations as measured using the gas analyzer based on the dry gas condition.

The result indicated that the concentration of produced gas increased sharply from zero within 1.5 min after methane was added to the reactor. At the end of the reduction reaction, the calculated exhaust methane flow rate was 0.15 LPM, and the CO_2 flow rate was 0.38 LPM. Excluding nitrogen and oxygen, the exhaust methane and CO_2 accounted for 28.4 and 71.6 v/v %, respectively, of the produced gas. CO and H_2 were not present in the exhaust gas.

From the definition of the fuel conversion rate, the methane conversion rate for this reducing process was calculated to be 71.6%. The reducing process of BOF slag was an endothermal reaction, and the temperature at the bottom of the reactor was observed to decrease from 950 to 942 °C.

After the reduction, the reactor was purged with nitrogen for 3 min. Subsequently, air with 18 v/v % of oxygen was introduced into the reactor at a flow rate of 6.5 LPM to oxidize the BOF slag; the oxidation lasted for 5 min. According to the gas analyzer data, carbon dioxide was absent, indicating that thermal decomposition of methane did not occur in the reducing process.

Figure 6a presents the oxygen concentration in the test. After more than 1 min, the oxygen concentration began increasing. Until the end of the oxidation process, the calculated oxygen flow rate and concentration were 0.62 LPM and 10.7%, respectively, indicating that the oxygen in the input air was consumed by the oxidation reaction. Furthermore, heat was released, causing the temperature at the bottom of the reactor to increase from 950 to 977 °C.

Subsequently, the influence of methane concentration on the reaction of BOF slag was analyzed using fuel with methane contents of 5 and 15 v/v %. Because the total input gas flow rate was controlled at 6.5 LPM, the methane flow rates with these methane contents were 0.32 and 0.97 LPM, respectively. Figure 6b,c present the calculated flow rates of CH_4, CO_2, and O_2 in the exhaust gas. For an input methane concentration of 5%, the exhaust methane and CO_2 flow rates were 0.08 and 0.16 LPM, respectively. For an input methane concentration of 15% v/v, the exhaust methane and CO_2 flow rates were 0.19 and 0.64 LPM, respectively. H_2 and CO were not observed in the exhaust gas; consequently, for methane input concentrations of 5 and 15 v/v %, the methane conversion rates were 65.8 and 76.6%, respectively. Because the reduction of the oxygen carrier was an endothermal reaction, a decrease in the reaction temperature was also measured.

After the reduction of the oxygen carrier, the reactor was purged using nitrogen, and compressed air with an oxygen concentration of 18 v/v % was introduced into the reactor at a flow rate of 6.5 LPM for the oxidation process of the oxygen carrier. The oxidation process lasted between 8 and 13 min. For a methane input concentration of 5 v/v %, the oxygen flow rate in the exhaust gas remained below 0.1 LPM for the initial 1 min because the oxidizing reaction consumed the oxygen. Subsequently, the oxygen flow rate and concentration increased to approximately 1.06 LPM and 17 v/v %, respectively.

For a methane input concentration of 15% (v/v), the oxygen flow rate in the exhaust gas continued to decrease in the initial oxidizing reaction because of the consumption of oxygen in the reaction. After approximately 12 min (i.e., the fourth minute of the reaction), the oxygen flow rate and concentration increased to approximately 0.83 LPM and 10 v/v %, respectively.

Because the oxidation process was an exothermal reaction, an increase in the reaction temperature was also measured. For methane input concentrations of 5 and 15 v/v %, the reaction temperature increased to approximately 963 and 987 °C, respectively.

Experiments with methane input concentrations of 5, 10, and 15% indicated that as the methane concentration increased, the effective collisions between methane and Fe_2O_3 contained in the oxygen carrier increased, resulting in the consumption of more methane to produce CO_2. Therefore, a higher methane input concentration resulted in a higher CO_2 concentration and a higher methane conversion rate.

4.2. Effect of the Reaction Temperature. The effect of temperature on the fluidized reaction of methane and BOF slag

https://doi.org/10.1021/acsomega.3c03390
ACS Omega 2023, 8, 47075−47085

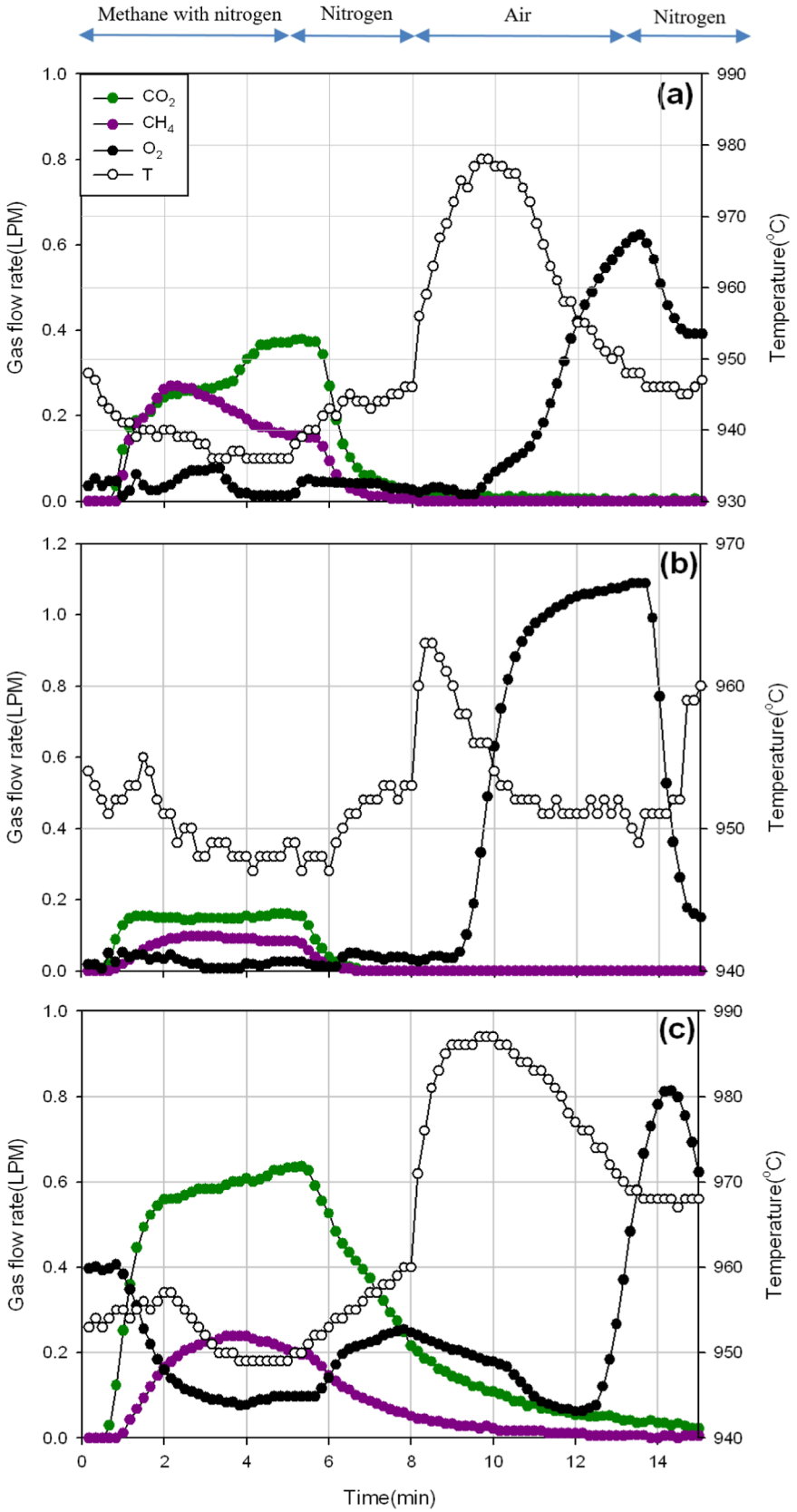

Figure 6. Produced gas composition, calculated flow rate, and temperature at the bottom of the reactor during the reduction−oxidation reaction of BOF slag and methane (a) test 1, (b) test 2, and (c) test 3; experimental conditions referring to Table 2.

was investigated at the fluidization and reaction test facility. The total input flow rate was set at 6.5 LPM, and the methane concentration and flow rate were 10 v/v % and 0.65 LPM, respectively, in the reduction process. The reactor was filled with 490 cm^3 of BOF slag, and the h/D value of the oxygen carrier was 5. For the reaction of methane and Fe_2O_3, the reaction

https://doi.org/10.1021/acsomega.3c03390
ACS Omega 2023, 8, 47075−47085

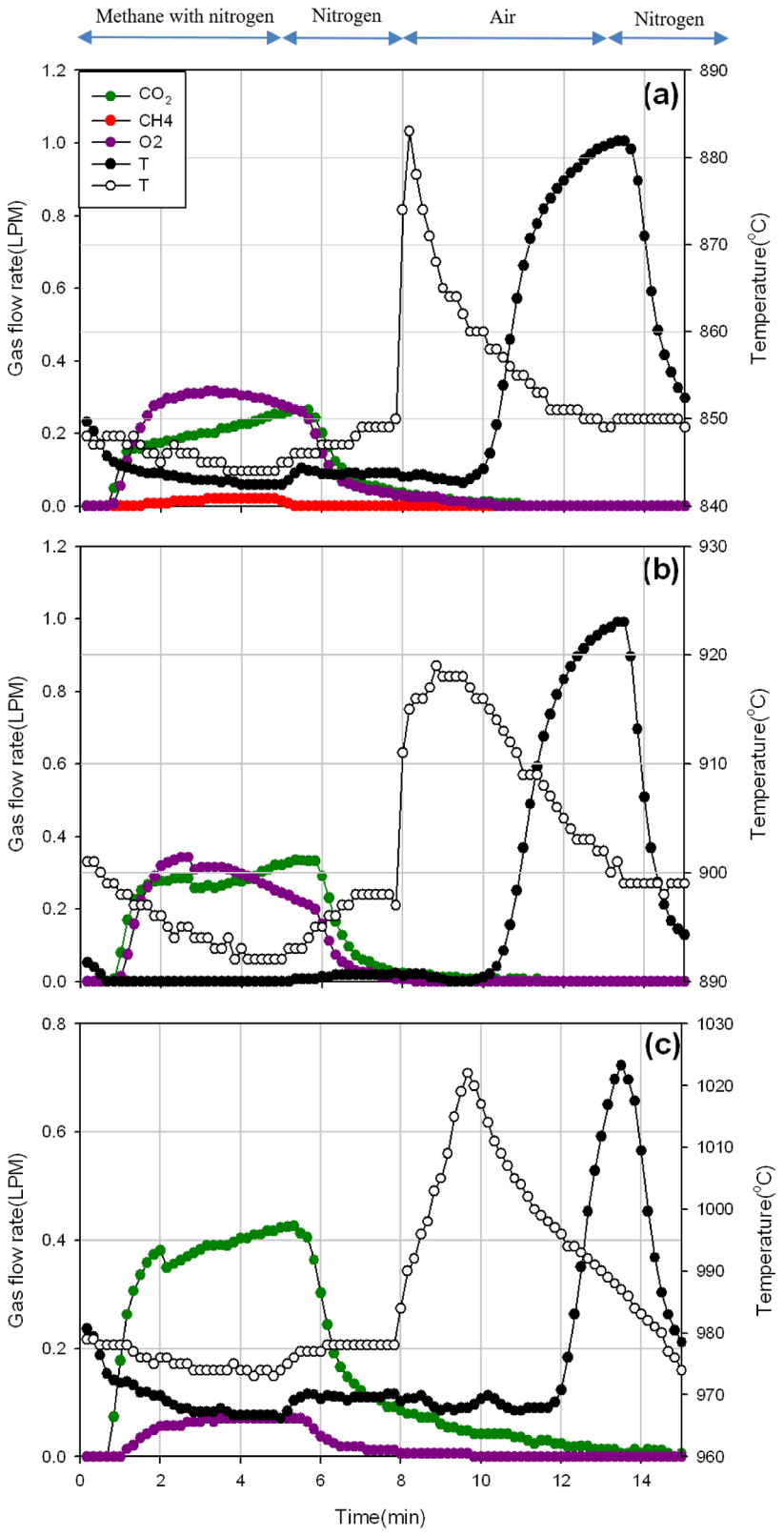

Figure 7. Produced gas composition, calculated flow rate, and temperature at the bottom of the reactor during the reduction−oxidization reaction of BOF slag and methane (a) test 4, (b) test 5, and (c) test 6; experimental conditions referring to Table 2.

temperature was controlled above 850 °C to achieve better conversion between the reactants. Specifically, the reaction temperature was set at 850, 900, 950 °C (test 1), and 980 °C.

Figure 7a illustrates the calculated flow rates of methane, CO_2, and O_2 in the exhaust gas at a reaction temperature of 850 °C. Within 2 min after methane input into the reactor, the concentration of the produced gas increased sharply from zero. At the end of the reducing process, the exhaust methane and CO_2 flow rates were 0.24 and 0.26 LPM, respectively. A small amount of H_2 was also produced, with a flow rate of 0.019

https://doi.org/10.1021/acsomega.3c03390
ACS Omega 2023, 8, 47075−47085

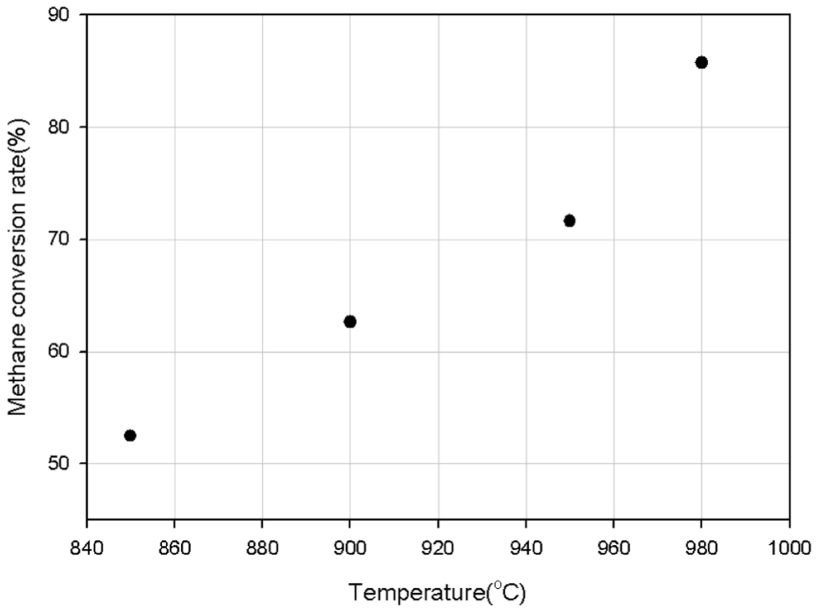

Figure 8. Correlation between the methane conversion rate and the reaction temperature (test 1, test 4−test 6).

LPM. With oxygen and nitrogen in the exhaust gas excluded, the methane and CO_2 concentrations were 47.5 and 52.5%, respectively, and the methane conversion rate was 52.5%. In the reduction process, the reaction temperature decreased owing to the endothermal reaction.

In the oxidation process, air was introduced into the reactor at a flow rate of 6.5 LPM. Then, the reaction temperature increased from 850 to 883 °C. Oxygen was consumed by the oxidizing reaction, and the flow rate remained close to 0 for approximately 2 min. As the oxygen carrier was almost oxidized, the oxygen flow rate and concentration increased to approximately 1 LPM and 16.2%, respectively.

Figure 7b illustrates the calculated flow rates of the exhaust gas species and the reactor temperature at a reaction temperature of 900 °C. After the concentration of produced gas increased sharply from zero, the methane and CO_2 flow rates in the exhaust gas were calculated to be 0.19 and 0.33 LPM, respectively. With the oxygen and nitrogen in the exhaust gas excluded and because CO and H_2 were absent, the methane and CO_2 concentrations were 37.4 and 62.6%, respectively, and the methane conversion rate was 62.6%.

Air was introduced into the reactor for the oxidation process. Oxygen was consumed by the oxidation reaction, and the oxygen concentration remained close to 0 for approximately 2 min. Meanwhile, the reaction temperature increased to approximately 920 °C owing to the exothermal reaction. When the oxygen carrier was almost oxidized, the oxygen flow rate and concentration increased to 1 LPM and 16%, respectively.

Figure 7c illustrates the calculated flow rates of the exhaust gas species at a reaction temperature of 980 °C. The methane and CO_2 flow rates were 0.42 and 0.07 LPM, respectively. With oxygen and nitrogen in the exhaust gas excluded and because CO and H_2 were absent, the methane and CO_2 concentrations were 14.3 and 85.7%, respectively, and the methane conversion rate was 85.7%. The reactor temperature exhibited an obvious decrease during this process because of the endothermal reduction reaction.

In the oxidation process, air was introduced into the reactor, and oxygen oxidized the oxygen carrier. Thus, heat was released, and the reactor temperature increased to 1020 °C. Because of the consumption of oxygen, the oxygen concentration in the exhaust gas remained close to 0. As the oxygen carrier was nearly completely oxidized, the oxygen flow rate and concentration increased to 0.72 LPM and 12.2%, respectively.

Figure 8 presents the correlation between the methane conversion rate and the reaction temperature. When the reaction temperature increased from 850 to 980 °C, the methane conversion rate linearly increased from 52.5 to 85.7%, respectively. This finding indicated that the reaction temperature played a crucial role in the conversion of fuel.

4.3. Effect of Gas Velocity. In the fluidization reaction of methane and the oxygen carrier, the input gas flow velocity influenced the fluidized state of the oxygen carrier and the gas residence time in the reactor. Gas always flowed into the reactor at a velocity above the minimum fluidization velocity to achieve adequate mixing between the gas and the oxygen carrier for fluidization. The high gas velocity resulted in a strong fluidized state (circulating and bubbling fluidization) of the oxygen carrier and made the oxygen carrier circulate in the interconnected fluidized-bed chemical looping system. However, it also reduced the gas residence time in the reactor and hampered the reaction between the gas and the oxygen carrier. To study the effect of the gas velocity on the fluidization reaction of methane and BOF slag, this study controlled the methane flow rate at 0.65 LPM for an oxygen carrier volume of 490 cm^3 and a h/D value of 5. Subsequently, the gas flow rates were controlled at 6.5 LPM (test 1), 5 LPM, and 3 LPM, with the gas velocities being 22.5, 17.3, and 10.4 cm/s (i.e., 5.1, 3.9, and 2.4 times the minimum fluidization velocity of BOF slag), respectively, for a reaction temperature of 950 °C.

Figure 9a presents the calculated flow rate of exhaust gas species and the reactor temperature at a gas flow rate of 5 LPM; the reaction reached a steady state in 2 min. The calculated methane and CO_2 flow rates in the exhaust gas were 0.09 and 0.32 LPM, respectively. With nitrogen and oxygen excluded and because CO and H_2 were absent, the methane and CO_2 concentrations were 23.5 and 76.5%, respectively, and the methane conversion rate was 76.5%.

Accordingly, in the oxidizing process, as air was introduced into the reactor, the exothermal oxidizing reaction between the

https://doi.org/10.1021/acsomega.3c03390
ACS Omega 2023, 8, 47075−47085

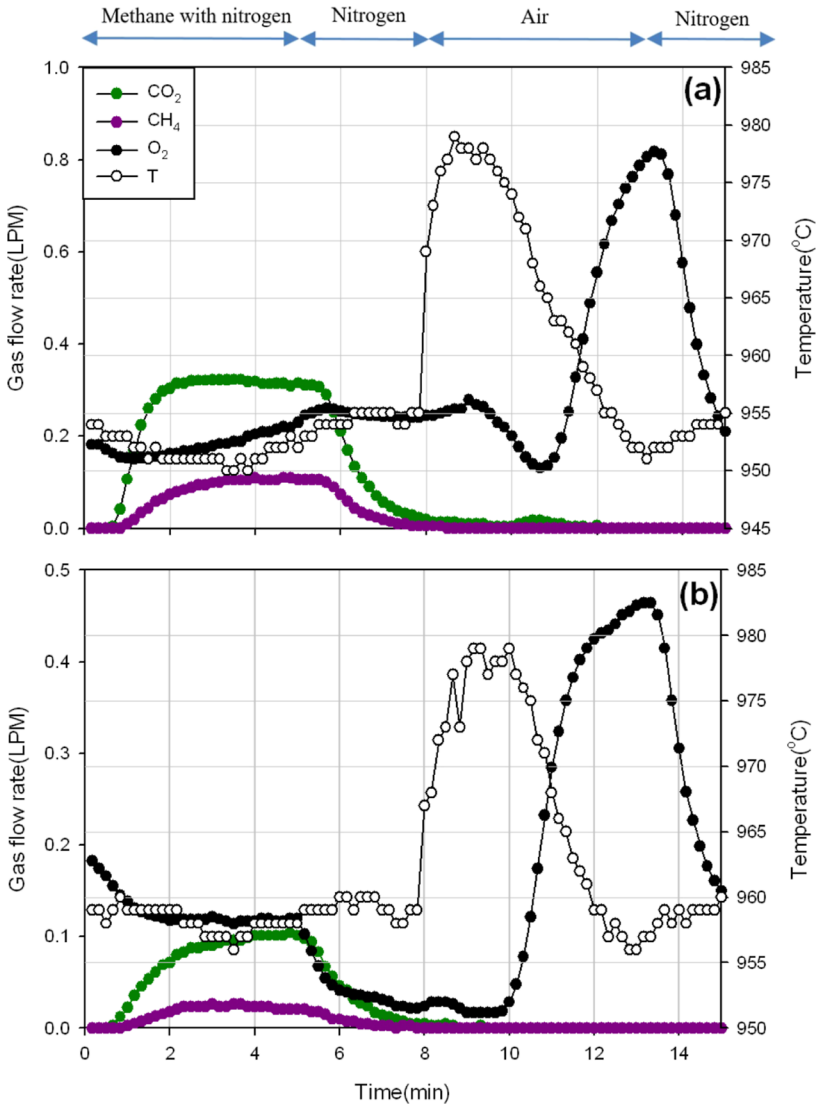

Figure 9. Produced gas composition, calculated flow rate, and temperature at the bottom of the reactor during reduction−oxidization; reaction of BOF slag and methane (a) test 7 and (b) test 8; experimental conditions referring to Table 2.

oxygen carrier and oxygen released heat, and the reactor temperature increased to 979 °C. At the start of the reaction, oxygen was consumed in the reaction, and the flow rate was below 0.1 LPM. After 11 min (i.e., the third minute of the oxidation reaction), the oxygen flow rate and concentration increased to 0.81 LPM and 15.8%, respectively.

At a gas flow rate of 3 LPM, the reaction reached a steady state in 3 min (Figure 9b). The calculated flow rates of methane and CO_2 were 0.02 and 0.1 LPM, respectively. Excluding nitrogen and oxygen, and because CO and H_2 were absent, the methane and CO_2 concentrations were 16.7 and 83.3%, respectively, and the methane conversion rate was 83.3%.

In the oxidizing process, as air was introduced into the reactor to react with the reduced oxygen carrier, heat was released, and the reactor temperature increased to 979 °C. Oxygen was consumed by the oxidation reaction, and the oxygen flow rate increased after 10 min (i.e., 3 min after air was introduced into the reactor). At the end of the process, the oxygen flow rate and concentration were 0.46 LPM and 16.5%, respectively.

The gas velocity influenced the fluidization state of the oxygen carrier and the gas residence time in the reactor. The lower the gas velocity, the smoother the fluidized state of the oxygen carrier and the longer the gas residence time, resulting in less mixing but a better reaction between the oxygen carrier and fuel gas. The test results of the effect of the flow velocity on the fluidization reaction of the BOF slag indicated that the gas velocity strongly influenced the fuel conversion rate. When the gas velocity was above the U_{mf} of the oxygen carrier, the methane conversion rate was enhanced as the flow velocity decreased. As the gas velocity decreased from 22.5 to 10.4 cm/s, the methane conversion rate increased from 71.1 to 83.3%.

4.4. Analysis of the BOF Slag Oxygen Carrier. At the end of the fluidization reaction test, the last process left was the reduction process. After this process, nitrogen was continuously purged, and the system was cooled. Subsequently, the reduced oxygen carrier from the experiments with high methane conversion rates was sampled to analyze the conversion rate. Table 3 lists the methane and oxygen carrier conversion rates in the experiments. Test 1 was performed with a 10 vol % methane concentration and a reaction temperature of 950 °C. An XRD analysis of the iron oxide (Figure 10) revealed the presence of Fe and Fe_3O_4. The oxygen carrier conversion rate of 9.6% indicated that almost all iron oxide was in the Fe_3O_4 state, with less in the FeO and Fe states. As FeO was cooled down from the reaction

https://doi.org/10.1021/acsomega.3c03390
ACS Omega 2023, 8, 47075−47085

Table 3. Conversion Rate of Methane and Oxygen Carriers of the Fluidized Reaction Tests

	methane conversion rate (%)	oxygen carrier conversion rate (%)
test 1	71.6	9.6
test 3	76.6	10.6
test 6	85.7	11.0
test 7	76.5	10.8
test 8	83.3	13.0

temperature to room temperature, it decomposed into Fe and Fe_3O_4.[29] Therefore, Fe was detected in the sample of test 1. Test 3 was performed with a 15% methane concentration, and it exhibited a higher methane conversion rate compared with that in test 1. The higher methane supply also resulted in a higher oxygen carrier conversion rate of 10.6%. An XRD analysis of the iron oxide revealed the presence of Fe and Fe_3O_4, indicating that almost all of the iron oxide was in the Fe_3O_4 state.

Test 6 was at the reaction temperature of 980 °C, and test 7 was performed with a lower gas velocity of 17.3 cm/s. These two experiments also showed a better methane conversion rate and oxygen carrier conversion rate than test 1. XRD analysis of the iron oxide revealed that most of it was in the Fe_3O_4 state, with a little in the Fe state.

Test 8 was performed with a gas velocity of 10.4 cm/s, which was 2.3 times the minimum fluidization velocity of the BOF oxygen carrier. The methane and oxygen carrier conversion rates increased to 83.3 and 13.0%, respectively. As the iron oxide conversion rate exceeded 11.1%, the iron state changed from Fe_3O_4 to FeO. An XRD analysis of the iron oxide revealed the presence of Fe and Fe_3O_4 with a prominent Fe signal, indicating that although most of the iron oxide was in the Fe_3O_4 state, a greater amount of Fe_2O_3 was reduced to FeO and Fe.

5. CONCLUSIONS

BOF slag is a byproduct of the steelmaking process. The iron content of BOF slag allows it to be used as an oxygen carrier in the chemical looping process and affords the advantage of reduced system operational costs. In order to develop a fluidized-bed chemical looping combustion system using BOF slag as the oxygen carrier, this paper studied the fluidization reaction properties of BOF slag and methane. The U_{mf} of BOF slag with a particle diameter of 177−297 μm was measured to be 4.4 cm/s at a h/D value of 5 in a batch fluidization and reaction test facility.

The fluidization and reaction hot mode tests showed that higher methane concentrations promoted the reaction between the oxygen carrier and methane and resulted in a higher conversion rate of methane. For an input methane concentration increased from 5 v/v % (test 2) to 15 v/v % (test 3), the methane conversion rate was promoted from 65.8 to 76.6%. Besides, as the reaction temperature increased from 850 °C (test 4) to 980 °C (test 6), the methane conversion rate increased from 52.6 to 85.7%, and in the exothermal oxidization process, the reactor temperature increased to 1020 °C.

The fluidization gas velocity influenced the fluidization conditions of the oxygen carrier and gas residence time in the reactor. As long as the gas velocity was above U_{mf} to ensure proper mixing between the oxygen carrier and methane, the reduced gas velocity increased the gas residence time in the reactor and facilitated both the reaction between the oxygen carrier and methane and the methane conversion. At test 1, the input gas velocity was 5.1 times U_{mf} of the oxygen carrier, and the methane conversion rate was 71.6%. When the gas velocity was reduced to 3.9 times (test 7) and 2.3 times (test 8) in the U_{mf} of the oxygen carrier, the methane conversion rate was improved to 76.5 and 83.3%, respectively. The lower gas velocity of test 8 also caused the oxygen carrier to have a higher conversion rate of

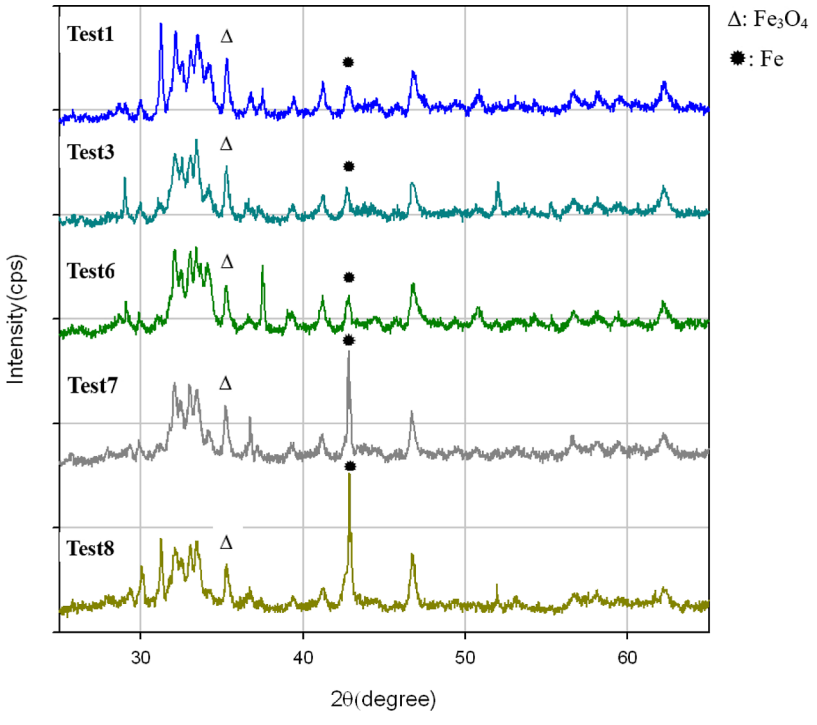

Figure 10. XRD patterns of oxygen carriers vented from the reducing process.

https://doi.org/10.1021/acsomega.3c03390
ACS Omega 2023, 8, 47075−47085

13%. Consequently, most of the iron in reduced BOF slag was in the Fe_3O_4 state, with a little in the Fe state.

This study demonstrated that the gas velocity, reaction temperature, methane concentration, and oxygen carrier supply all influence the fluidization reaction between the fuel gas and oxygen carrier in the fluidized-bed chemical looping system. The test results could be used to optimize the design of the reactor geometry and the operational parameters of the interconnected fluidized-bed chemical looping system.

AUTHOR INFORMATION

Corresponding Author

Cetera Chen − *Green Energy and Environment Research Laboratories, Industrial Technology Research Institute, Hsinchu 31040, Taiwan, (R.O.C.)*; orcid.org/0000-0002-7928-7037; Email: Cetera.Chen@itri.org.tw

Authors

Seng-Rung Wu − *Green Energy and Environment Research Laboratories, Industrial Technology Research Institute, Hsinchu 31040, Taiwan, (R.O.C.)*

Ching-Ti Kao − *Green Energy and Environment Research Laboratories, Industrial Technology Research Institute, Hsinchu 31040, Taiwan, (R.O.C.)*

Complete contact information is available at: https://pubs.acs.org/10.1021/acsomega.3c03390

Notes

The authors declare no competing financial interest.

ACKNOWLEDGMENTS

This research is supported by the Bureau of Energy, Ministry of Economic Affairs, Republic of China (ROC).

REFERENCES

(1) Republic of China government. Greenhouse Gas Reduction and Management Action, 2015.

(2) Notz, R.; Tonnies, I.; McCann, N.; Scheffknecht, G.; Hasse, H. CO_2 Capture for Fossil Fuel Fired Power Plants. *Chem. Eng. Technol.* **2011**, *34* (2), 163−172.

(3) Ennenbach, F.; Kluger, K. Challenges for 2nd Generation Technologies Like Chemical and Carbonate Looping from an Industry Point of View. *Proceedings of 2nd International Conference of Chemical Looping, Darmstadt, Germany*, 2012.

(4) Abad, A.; Adánez, J.; García-Labiano, F.; de Diego, L. F.; Gayán, P.; Celaya, J. Mapping of the Range of Operational Conditions for Cu-Fe-and Ni-based Oxygen Carriers in Chemical-looping Combustion. *J. Chem. Eng. Sci.* **2007**, *62*, 533−549.

(5) Forero, C. R.; Gayán, P.; de Diego, L. F.; Abad, A.; García-Labiano, F.; Adánez, J. Syngas Combustion in a 500W_{th} Chemical-looping Combustion System Using an Impregnated Cu-based Oxygen Carrier. *Fuel Process. Technol.* **2009**, *90*, 1471−1479.

(6) Johansson, M.; Mattisson, T.; Lyngfelt, A. Use of $NiO/NiAl_2O_4$ Particles in a 10 kW Chemical-looping Combustor. *Ind. Eng. Chem. Res.* **2006**, *45*, 5911−5919.

(7) Figueroa, J. D.; Fout, T.; Plasynski, S.; McIlvried, H.; Srivastava, R. D. Advances in CO_2 Capture Technology-The U.S. Department of Energy's Carbon Sequestration Program. *Int. J. Greenhouse Gas Control* **2008**, *2*, 9−20.

(8) Euroslag, Statistics, 2008 http://www.euroslag.org/products/statistics/2008/.

(9) Geiseler, J. Use of steelworks slag in Europe. *Waste Manage.* **1996**, *16*, 59−63.

(10) Proctor, D. M.; Fehling, K. A.; Shay, E. C.; Wittenborn, J. L.; Green, J. J.; Avent, C.; Bigham, R. D.; Connolly, M.; Lee, B.; Shepker, T. O.; Zak, M. A. Physical and Chemical Characteristics of Blast Furnace, Basic Oxygen Furnace, and Electric Arc Furnace Steel Industry Slags. *Environ. Sci. Technol.* **2000**, *34*, 1576−1582.

(11) Ryden, M.; Cleverstam, E.; Lyngfelt, A.; Mattisson, T. Waste Products from the Steel Industry with NiO as Additive as Oxygen Carrier for Chemical-looping Combustion. *Int. J. Greenh. Gas Control* **2009**, *3*, 693−703.

(12) Zeng, L.; Tong, A.; Kathe, M.; Bayham, S.; Fan, L.-S. Iron Oxide Looping for Natural Gas Conversion in a Countercurrent Moving Bed Reactor. *Appl. Energy* **2015**, *157*, 338−347.

(13) Chen, C.; Lee, H. H.; Chen, W.; Chang, Y. C.; Wang, E.; Shen, C. H.; Huang, K. E. Study of an Iron-Based Oxygen Carrier on the Moving Bed Chemical Looping System. *Energy Fuels* **2018**, *32*, 3660−3667.

(14) Linderholm, C.; Lyngfelt, A.; Cuadrat, A.; Jerndal, E. Chemical-looping Combustion of Solid Fuels - Operation in a 10 kW Unit with Two Fuels, Above-bed and In-bed Fuel Feed and Two Oxygen Carriers, Manganese Ore and Ilmenite. *Fuel* **2012**, *102*, 808−822.

(15) Hildor, F.; Leion, H.; Linderholm, C. J.; Mattisson, T. Steel Converter Slag as an Oxygen Carrier for Chemical-looping Gasification. *Fuel Process. Technol.* **2020**, *210*, 106576.

(16) Wang, P.; Leion, H.; Yang, H. Oxygen-Carrier-Aided Combustion in a Bench-Scale Fluidized Bed. *Energy Fuels* **2017**, *31*, 6463−6471.

(17) Ryden, M.; Hanning, M.; Lind, F. Oxygen Carrier Aided Combustion (OCAC) of Wood Chips in a 12 MW_{th} Circulating Fluidized Bed Boiler Using Steel Converter Slag as Bed Material. *Appl. Sci.* **2018**, *8*, 2657.

(18) Moldenhauer, P.; Linderholm, C.; Ryden, M.; Lyngfelt, A. Avoiding CO_2 Capture Effort and Cost for Negative CO_2 Emissions Using Industrial Waste in Chemical-looping Combustion/gasification of Biomass. *Mitig. Adapt. Strategies Glob. Change* **2020**, *25*, 1−24.

(19) Mattison, T.; Hildor, F.; Li, Y.; Linderholm, C. Negative Emissions of Carbon Dioxide Through Chemical-looping Combustion (CLC) and Gasification (CLG) Using Oxygen Carriers Based on Manganese and Iron. *Mitig. Adapt. Strategies Glob. Change* **2020**, *25*, 497−517.

(20) Hildor, F.; Mattisson, T.; Leion, H.; Linderholm, C.; Ryden, M. Steel Converter Slag as an Oxygen Carrier in a 12 MW_{th} CFB Boiler-Ash Interaction and Material Evolution. *Int. J. Greenh. Gas Control* **2019**, *88*, 321−331.

(21) Qin, L.; Majumder, A.; Fan, J. A.; Kopechek, D.; Fan, L.-S. Evolution of Nanoscale Morphology in Single and Binary Metal Oxide Microparticles During Reduction and Oxidation Processes. *J. Mater. Chem. A* **2014**, *2*, 17511−17520.

(22) Qin, L.; Cheng, Z.; Fan, J. A.; Kopechek, D.; Xu, D.; Deshpande, N.; Fan, L.-S. Nanostructure Formation Mechanism and Ion Diffusion in Iron-titanium Composite Materials with Chemical Looping Redox Reactions. *J. Mater. Chem. A* **2015**, *3*, 11302−11312.

(23) Kao, C.-T.; Shen, C.-H.; Hsu, H.-W. Feasibility Study of an Iron-Based Composite Added withAl_2O_3/ZrO_2 as an Oxygen Carrier in the Chemical Looping Applications. *Crystal* **2021**, *11*, 971.

(24) Ergun, S. Fluid Flow Through Packed Columns. *Chem. Eng. Prog.* **1952**, *8* (2), 89−94.

(25) Pata, J.; Hartman, M. Minimum Fluidization Velocities of Lime and Limestone Particles. *Ind. Eng. Chem. Process Des. Dev.* **1978**, *17* (3), 231−236.

(26) Liu, X.; Xu, G.; Gao, S. Micro fluidized beds: Wall effect and operability. *Chem. Eng. J.* **2008**, *137*, 302−307.

(27) Rao, A.; Curtis, J. S.; Hancock, B. C.; Wassgren, C. The Effect of Column Diameter and Bed Height on Minimum Fluidization Velocity. *Am. Inst. Chem. Eng.* **2010**, *56* (9), 2304−2311.

(28) Miller, D. D.; Siriwardane, R.; Poston, J. Fluidized-bed and Fixed-bed Reactor Testing of Methane Chemical Looping Combustion with MgO-promoted Hematite. *Appl. Energy* **2015**, *146*, 111−121.

(29) Chen, C.; Chen, C.-H.; Chang, M.-H.; Lee, H.-H.; Chang, Y.-C.; Wen, T.-W.; Shen, C. H.; Wan, H. P. 30-kW_{th} Moving-Bed Chemical Looping System for Hydrogen Production. *Int. J. Greenh. Gas Control* **2020**, *95*, 102954.